Nanotechnology **20** (2009) 345701 (7pp) doi:10.1088/0957-4484/20/34/345701

The optoelectronic properties of a photosystem I–carbon nanotube hybrid system

Simone M Kaniber[1,2], Friedrich C Simmel[2,3], Alexander W Holleitner[1,2] and Itai Carmeli[4,5]

[1] Walter Schottky Institut, Technische Universität München, Am Coulombwall 3, D-85748 Garching, Germany
[2] LMU Munich, Geschwister-Scholl-Platz 1, D-80539 München, Germany
[3] Physik Department, Technische Universität München, James Franck Straße 1, D-85748 Garching, Germany
[4] Chemistry Department and NIBN, Ben Gurion University, 84105 Be'er Sheva, Israel
[5] Department of Chemistry and Biochemistry, Tel-Aviv University, 69978 Tel-Aviv, Israel

E-mail: holleitner@wsi.tum.de and itai@post.tau.ac.il

Received 19 January 2009, in final form 6 July 2009
Published 4 August 2009
Online at stacks.iop.org/Nano/20/345701

Abstract
The photoconductance properties of photosystem I (PSI) covalently bound to carbon nanotubes (CNTs) are measured. We demonstrate that the PSI forms active electronic junctions with the CNTs, enabling control of the CNTs' photoconductance by the PSI. In order to electrically contact the photoactive proteins, a cysteine mutant is generated at one end of the PSI by genetic engineering. The CNTs are covalently bound to this reactive group using carbodiimide chemistry. We detect an enhanced photoconductance signal of the hybrid material at photon wavelengths resonant to the absorption maxima of the PSI compared to non-resonant wavelengths. The measurements prove that it is feasible to integrate photosynthetic proteins into optoelectronic circuits at the nanoscale.

(Some figures in this article are in colour only in the electronic version)

1. Introduction

Photosynthetic reaction centers are the photochemically active complexes in photosynthetic systems found in plants, algae and photosynthetic bacteria [1]. The photosynthetic reaction centers have evolved approximately 3.5 billion years ago, and they serve as the ultimate source of energy in the biosphere. Photosystem I (PSI) has a cylindrical shape with a diameter of about 15 nm and a height of 9 nm [1], and it is composed of polypeptide chains in which chlorophyll and carotenoids are embedded (figure 1(a)). The photosynthetic process involves an efficient conversion of solar energy to stable chemical energy. Following photo-excitation, an electron is transferred along an electron transfer pathway within the protein complex (depicted in red, figure 1(a)) from the lumen to the stroma side of the PSI. The final acceptors are located about 6 nm away from the initially oxidized reaction-center chlorophyll P700. During this process the reaction-center photosystem I (PSI) acts as a nanosized photodiode composed of a protein chlorophyll complex that utilizes light to generate a photopotential of about 1 V with a quantum efficiency of 1 and an intrinsic energy conversion efficiency of 58% (47% of the total absorbed light) [2–7]. Recently, we have demonstrated the possibility to covalently bind the PSI reaction center directly to gold surfaces [4] as well as indirectly via a small linker molecule to GaAs surfaces [8] and to single- and multi-walled carbon nanotubes (CNTs) [3]. Additionally, self-assembled monolayers (SAMs) of PSI on gold electrodes can be contacted by CNTs [3]. Initial evidence demonstrated that this SAM device shows an enhanced photoconductance signal due to PSI [3].

The present study investigates the optoelectronic properties of hybrids made of the PSI and single-walled CNTs in greater detail. CNTs are rolled-up graphene sheets along a

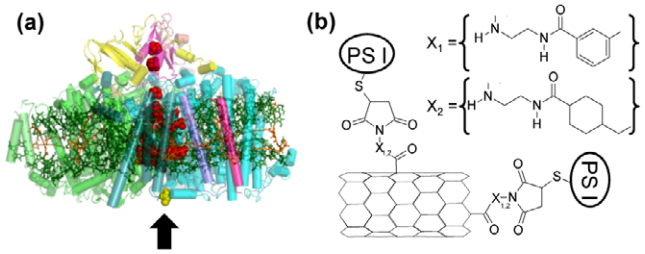

Figure 1. (a) Molecular structure image of photosystem I (PSI). The PSI covalently binds to maleimide-modified carbon nanotubes through a cysteine mutation on the polypeptide backbone (black arrow) which is close to the chromophores that mediate the electron transfer (represented by the space filling model). (b) Scheme of a nanoscale hybrid composed of carbon nanotubes (CNTs) and the (PSI). The sulfur-containing cysteine group of a mutant PSI binds covalently to a carboxylated CNT via a maleimide linker [3].

chiral vector [9] and, depending on this vector, they exhibit either semiconducting or metallic properties. Since the diameter of single-walled CNTs is in the range of 1–2 nm [10], CNTs seem to be the system of choice to electrically contact the PSI by covalently binding these proteins to the CNTs. The functionalization of CNTs by chemical modifications holds interesting prospects in various fields such as nucleic acid sensing [11] and the fabrication of hybrid bioorganic nanosystems [12–17]. In particular, it has been demonstrated how to covalently bind DNA [13] and nanocrystals [14, 15, 18–20] to CNTs, as well as CNTs to the end of an AFM tip [21]. Here, PSI–CNT hybrids are characterized by photoconductance measurements as a function of the excitation wavelength, the laser chopper frequency and the excitation location with respect to the gold contacts [22]. We detect a strongly enhanced photoconductance signal of the hybrid material between the metal contacts at photon wavelengths resonant with the absorption maxima of the PSI compared to non-resonant wavelengths. We do not observe such an enhanced photoconductance signal in control samples consisting merely of purified CNTs. We consider charge and energy transfer processes from the PSI to the CNTs in order to explain the observed photoconductance response of the PSI–CNT hybrid system [23]. We further rule out photodesorption effects on the surface of the CNTs [24], the effect of Schottky contacts between the CNTs and the metal contacts [22], electron–hole effects only within the CNTs [25–30] and bolometric effects [31] to dominate the photoconductance properties of the PSI–CNT hybrids. The results indicate that the integrated proteins are optoelectronically active and that the electron transfer chain within the PSI can be electronically contacted by CNTs. This study demonstrates that the PSI has the potential to be integrated in nanoscale solar or power cells, and the electrical addressing via CNTs is a first step in this direction. Namely, the excellent optical and electronic properties of CNTs qualify them as promising building blocks for nanoscale optoelectronic devices [10, 32–39] and the length of CNTs of up to several microns make them suitable as mesoscopic electrodes for the PSI as well as nanocrystals [40] and molecules [41, 42].

2. Materials and methods

2.1. Material and synthesis

The synthesis of the PSI–CNT hybrid system is done according to [3] as follows. First, the CNTs (Rice Company Inc.) are functionalized with carboxyl groups by refluxing in 3 M HNO_3 for 20 h (CNT concentration: approx. 0.9 mg l^{-1}). This acid treatment also cleans the CNTs. For an additional separation from smaller particles the CNT solution is diluted in 1 l deionized water with 0.2% Triton-X (Sigma-Aldrich) and filtered several times through a 0.1 μm PTFE filter (Millipore). Afterwards the CNTs are dialyzed for three days in bags (from Spectra Por float-A-lyser MW cutoff 10 000). In the second step amine reactive NHS-esters are generated at the carboxyl groups of the CNTs. For that, a suspension of the carboxylated CNTs (approx. 0.2 mg ml^{-1}) is sonicated for 1 h at room temperature in 0.1 M MES buffer pH 5 and 0.2% Triton-X together with 5 mM of 1-ethyl-3-(3-dimethyl amino-propyl) carbodiimide (EDC, Pierce) and 5 mM Sulfo-NHS (Pierce) [3]. Now 5 mM of ethylenediamine (EDA, Pierce) is reacted with 5 mM of Sulfo-MBS (Pierce) in 0.1 M PBS buffer pH 7.2 for 2 h at room temperature and added to the amine-reactive CNTs. The solution is stirred for another two hours and afterwards washed from the excess reagents. In the last step the PSI is covalently bound to the maleimide-functionalized CNTs (figure 1(b)). The functional groups on the PSI are amino acids in the extra membrane loops of the PSI facing the lumen side of the bacterial membrane (oxidizing side) which are mutated to cysteines (Cys) as described in [4]. The mutations D235C/Y634C are selected near the special chlorophyll pair P700, indicated by the black arrow in figure 1(a), to allow close proximity between the reaction center and the CNTs. These mutations do not have steric hindrance when placed on a solid state surface [4, 8] or CNTs [3]. After activation of the thiol Cys in PSI (typically 0.5 mg chlorophyll ml^{-1}) by reacting with dithiothreitol (Sigma-Aldrich) (2 mM) for 10 min at room temperature, 100 μl of the PSI (cleaned from excess reagent as in [3]) is added to 2 ml of the maleimide-modified CNTs (in 0.1 M PBS buffer, pH 7.2 and 0.2% Triton-X) and stirred for 2 h at room temperature. Afterwards, unbound proteins are removed by several centrifugation steps followed by suspending the functionalized CNTs again in the 0.1 M PBS buffer solution.

In a previous study [3] we demonstrated a similar four-step chemical route utilizing sulfo-SMCC (sulfosuccinimidyl 4-[*N*-maleimidomethyl] cyclohexane-1-carboxylate) instead of sulfo-MBS (m-maleimidobenzoyl-*N*-hydroxysulfosuccinimide ester from Pierce) which results in a linker molecule that has a cyclohexane instead of an aromatic hydrocarbon (figure 1(b)). We find that the difference between the two linker molecules does not result in modifications of the optoelectronic properties of the hybrid systems. Most importantly, the covalent binding of the Cys mutations located at the lumen side of the PSI to the CNTs gives rise to a unique topology of the PSI–CNT hybrids for optoelectronic applications. In this configuration, the oxidizing side of the PSI is oriented towards the CNTs. Our assembly approach facilitates efficient electronic junctions and avoids disturbance of the function of the reaction center.

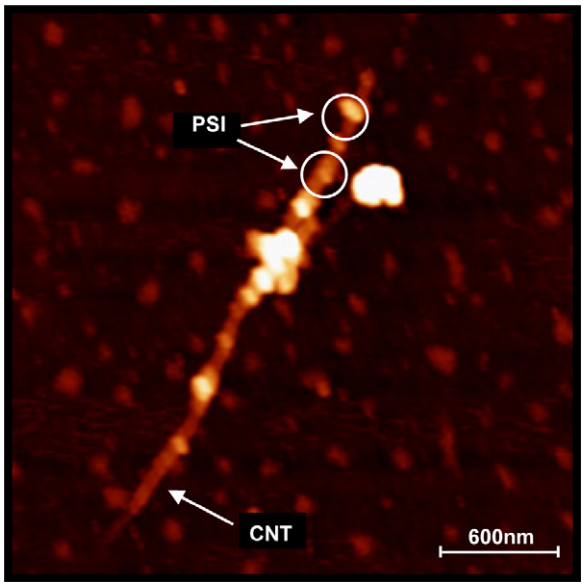

Figure 2. Atomic force micrograph (AFM) of PSI–CNT hybrids. The image shows a large number of PSI (circles) with diameters of about 9–20 nm bound to the tips and the side-walls of a CNT bundle [3].

The covalent attachment of the PSI through the Cys further ensures the structural stability of the assembled, oriented PSI–CNT hybrids.

2.2. AFM characterization of PSI–CNT hybrids

To evaluate the degree of conjugation between the modified CNTs and PSI, a drop of the solution with a concentration of PSI-functionalized CNTs of typically 0.02 g ml^{-1} is placed onto a silicon surface and incubated for 2 h at room temperature. The sample is washed briefly with deionized water and dried under nitrogen. Figure 2 shows an atomic force micrograph (AFM) of a PSI–CNT hybrid on a silicon surface. The image exhibits a large number of spherical particles (circles in figure 2) attached to the surface of the CNTs. The height analysis of the AFM images indicates a height of about 9–20 nm for the spherical particles (data not shown), in agreement with the actual diameter of the PSI, which suggests that the spherical particles are the PSI proteins [3]. The diameters of the CNTs are in the range of a few up to 6 nm. Single-walled CNTs typically have diameters of about 1–2 nm [31], while a height of 6 nm suggests that bundles of CNTs build the backbone of the PSI–CNT hybrids [43].

2.3. Photoconductance measurements

We electronically contact ensembles of PSI–CNT hybrids and purified CNTs by depositing a drop of an aqueous solution, which contains either PSI–CNT hybrids or purified CNTs, onto an insulating SiO_2 substrate with opto-lithographically predefined gold on top [40]. The concentration of the purified or PSI-functionalized CNTs is typically 0.3 mg ml^{-1} in H_2O. After drying at room temperature the chip is rinsed with deionized water and dried under nitrogen. The metal contacts,

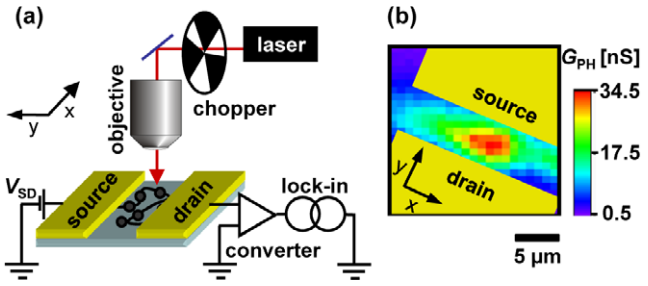

Figure 3. (a) Experimental circuit for measuring the photoconductance of PSI–CNT hybrids as a function of the spatial coordinates x and y. (b) Spatially resolved photoconductance signal at room temperature of an ensemble of PSI–CNT hybrids, which electronically bridge metal source–drain contacts with a distance of about 5 μm ($\lambda = 420$ nm).

which have a distance of 5–10 μm, are electronically bridged by the hybrids after drying. Because the area of the dried hybrid nanosystems is smaller than the metal contacts, the contacts act as source–drain electrodes for the PSI–CNT hybrids in a two-terminal configuration (sketch in figure 3(a)).

The photoconductance $G_{PH}(\lambda, f_{CHOP})$ of the hybrids is measured as a function of the photon wavelength λ, the chopper frequency f_{CHOP} and the location of the laser excitation with respect to the source–drain contacts (see the sketch of the experimental circuit in figure 3(a)). To this end, a bias voltage V_{SD} is applied across the source–drain electrodes, while the light of a titanium:sapphire laser is focused through an objective of a microscope onto the hybrid nanostructures. The current across the sample is fed through a current–voltage converter. A lock-in amplifier provides a dc signal of the current difference $\Delta I = I_{ON} - I_{OFF}$ across the sample for the laser being 'on' or 'off'. For a modulation frequency below 2 kHz, the necessary reference trigger is given by the chopper frequency f_{CHOP} of the chopper wheel (figure 3(a)). For photoconductance measurements at 76 MHz, we utilize the repetition frequency of the mode-locked titanium:sapphire laser. In both cases, the resulting ΔI can be translated into a photoconductance $G_{PH} = \Delta I / V_{SD} = G_{PH}(\lambda, f_{CHOP})$ of the electronically contacted nanosystem because the measured samples show an ohmic behavior at small V_{SD}. The zero potential of the current–voltage converter ensures that the source–drain voltage V_{SD} only drops across the sample. The conductance G is defined by $G = I / V_{SD}$. The location of the objective and thus the laser excitation with respect to the source–drain contacts can be controlled by piezo-positioners at a step size of about 50 nm. We utilize the current–voltage converter (lock-in) Ithaco 1211 (eg&g 7260) at frequencies below 2 kHz and a FEMTO HCA-100M_50K-C (Stanford Research SR 844) at a frequency of 76 MHz.

2.4. Absorbance measurements

The absorbance of the PSI is measured spectrally resolved with a Jasco V-550 UV–vis spectrophotometer. The absorption intensity for samples containing typically 5 μg chlorophyll ml^{-1} PSI in 20 mM tricine buffer (pH 7.7) are measured and

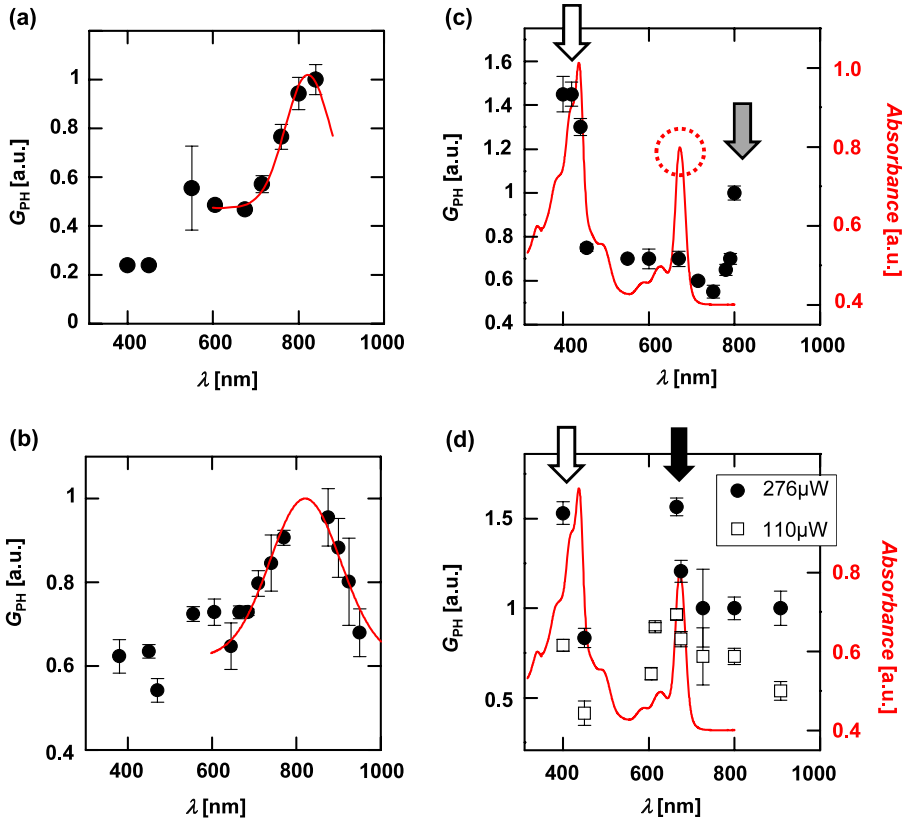

Figure 4. (a) Normalized photoconductance of purified CNTs as a function of the photon wavelength λ at $f_{CHOP} = 1.1$ kHz and $I_{LASER} = 32$ kW cm^{-2} at room temperature [43]. (b) Normalized photoconductance spectrum of pristine CNTs measured at 76 MHz and $I_{LASER} = 28$ kW cm^{-2}. The lines in (a) and (b) are Gaussian fits to the data with a center wavelength of 822 and 821 nm. (c) Normalized photoconductance of the PSI–CNT hybrids at $f_{CHOP} = 1.1$ kHz and $I_{LASER} = 6.4$ kW cm^{-2}. (d) Normalized photoconductance data on the same sample as in (c) at 76 MHz and $I_{LASER} = 35$ and 14 kW cm^{-2} (open squares: 110 μW and filled circles: 276 μW). Lines in (c) and (d): normalized absorbance of PSI in a buffer solution. See text for details.

20 mM pristine tricine buffer solution (pH 7.7) serves as the background.

3. Experimental results

3.1. Ruling out effects caused by photodesorption and Schottky barriers

There are several processes which can alter the photoconductance of the PSI–CNT hybrids, such as photodesorption effects on the surface of the CNTs [24], the effect of Schottky contacts between the CNTs and the gold contacts [22], electron–hole effects within the CNTs [25–30], bolometric effects [31] and charge as well as energy transfer processes within the PSI–CNT hybrids [23]. First, all of the samples are measured in vacuum ($p < 1 \times 10^{-3}$ mbar). Hereby, photodesorption effects can be ruled out, where the laser excitation would induce oxygen desorption of the dopant oxygen from the side-walls of the CNTs [24]. To rule out the effect of a Schottky barrier between the CNTs and the gold contacts as the dominating optoelectronic effect, the photoconductance of ensembles of PSI–CNT hybrids is measured, while the excitation spot is scanned in the directions x and y with respect to the source–drain contacts (figures 3(a) and (b)). The photoconductance exhibits a maximum in the center of the source and drain contacts at a distance of about 2 μm away from the metal contacts (figure 3(b)). Since Schottky barriers only emerge in close vicinity to the metal contacts, the data of figure 3(b) are evidence that Schottky barriers do not dominate the photoconductance in the present PSI–CNT hybrids. Comparing the spatial dependence of several PSI–CNT hybrid samples it can be determined that, in all cases, the signal is observed at positions where ensembles of dried PSI–CNT hybrids are located.

3.2. Wavelength-dependent photoconductance

In figures 4(a) and (b), the normalized photoconductance G_{PH} of an ensemble of purified CNTs without PSI is depicted as a function of the excitation wavelength[6]. A maximum of G_{PH} is found at about $\lambda = 822 \pm 11$ nm (lines are Gaussian fits to the experimental data). Following recent reports [25–30], the finding in figures 4(a) and (b) can be interpreted such that electron–hole dynamics in the semiconducting CNTs of the ensemble give rise to the observed photoconductance. A wavelength of $\lambda = 822 \pm 11$ nm translates into an intersubband transition $E_{22} = 1.51 \pm 0.16$ eV of a semiconducting single-walled CNT with a diameter of $d = 1.11 \pm 0.06$ nm (and

[6] In figures 3(a) and (b) ((c) and (d)) G_{PH} is normalized with respect to $G_{PH}(\lambda = 822$ nm) ($G_{PH}(\lambda = 800$ nm)).

$E_{11} = 0.77 \pm 0.07$ eV) [44]. We would like to note that the derived diameter of the CNTs is consistent with Raman data on the same set of CNTs (data not shown). Because the absorption cutoff of the PSI is around 700 nm (∼1.77 eV), the absorption corresponding to the E_{22} transition in the CNTs are detected in the photoconductance signal of the PSI–CNT hybrids at a photon wavelength larger than 700 nm as well, but they are not assigned to any contributions from the PSI. Indeed, for $\lambda > 780$ nm the photoconductance signal of the PSI–CNT hybrids rises for a longer wavelength (gray arrow in figure 4(c)). Intriguingly, for $\lambda < 450$ nm, a generally enhanced photoconductance signal of the PSI–CNT hybrids is detected (open arrow in figure 4(c)) as compared to the findings for the CNTs. The red line in figure 4(c) depicts the absorbance spectrum of the PSI (measured with the proteins being suspended in a buffer solution, see section 2.4). Typical for PSI, the chlorophyll absorbance maxima are at ∼440 and 680 nm [1]. The photoconductance increase for $\lambda < 450$ nm in figure 4(c) can be interpreted such that, at these wavelengths, the signal is dominated by the contribution of the chlorophylls in the PSI–CNT hybrids (open arrow in figure 4(c)). At 680 nm, the photoconductance is still enhanced as compared to the signal at $\lambda \sim 780$ nm. However, it is slightly suppressed as expected from the absorbance spectrum (dashed circle). Generally, figure 4(c) depicts photoconductance data for f_{CHOP} in the kHz regime. At a trigger frequency of 76 MHz for the lock-in amplifier (see section 2.3), the photoconductance signal of the PSI–CNT hybrids is enhanced again for $\lambda < 450$ nm (open arrow in figure 4(d)). Most importantly, however, an additional maximum at 680 nm can be resolved (black arrow in figure 4(d)). This maximum is not detected for purified CNTs at 1.1 kHz (figure 4(a)) and 76 MHz (figure 4(b)). We interpret the finding such that the optoelectronic response of the PSI–CNT hybrids happens on a fast timescale at 680 nm. As described in section 2.3, G_{PH} measures the difference of the conductance between the 'on' and 'off' states of the laser, and thereby it is sensitive to processes occurring at the chopper frequency.

3.3. Chopper frequency dependence of the photoconductance in the kHz regime

Figure 5(a) shows a typical frequency dependence of the photoconductance of the PSI–CNT hybrids in the kHz regime. For all λ and within the experimental error, no frequency dependence of the photoconductance is found for both the PSI–CNT hybrids and the purified CNT samples at a chopper frequency up to 2 kHz. Thus, photoconductance dynamics within the PSI–CNT hybrids in the millisecond timescale can be excluded ($1/(2\ \mathrm{kHz}) = 0.5$ ms) [20]. In turn, bolometric effects due to a change of the lattice temperature within the CNTs can be ruled out to dominate the photoconductance in the CNTs because such bolometric effects occur on the millisecond timescale [20, 31].

3.4. Lab time dependence of the conductance and the photoconductance

Figure 5(b) demonstrates that there are charge carrier dynamics within the PSI–CNT hybrids, which occur on a timescale of seconds and longer. The upper graph of figure 5(b) depicts the photoconductance G_{PH} of the PSI–CNT hybrids as a function of the laboratory time. As noted above, whenever the laser is switched on, a constant photoconductance signal is measured (shaded area in figure 5(b)), while if it is switched off there is no signal G_{PH} detected. As can be viewed in the lower graph of figure 5(b), after the laser excitation a stepwise change in G with a timescale of several seconds is observed (see the exponential fit in the lower graph of figure 5(b)). The conductance G reaches the value of the initial state only after the PSI–CNT hybrids having been in darkness for several hours.

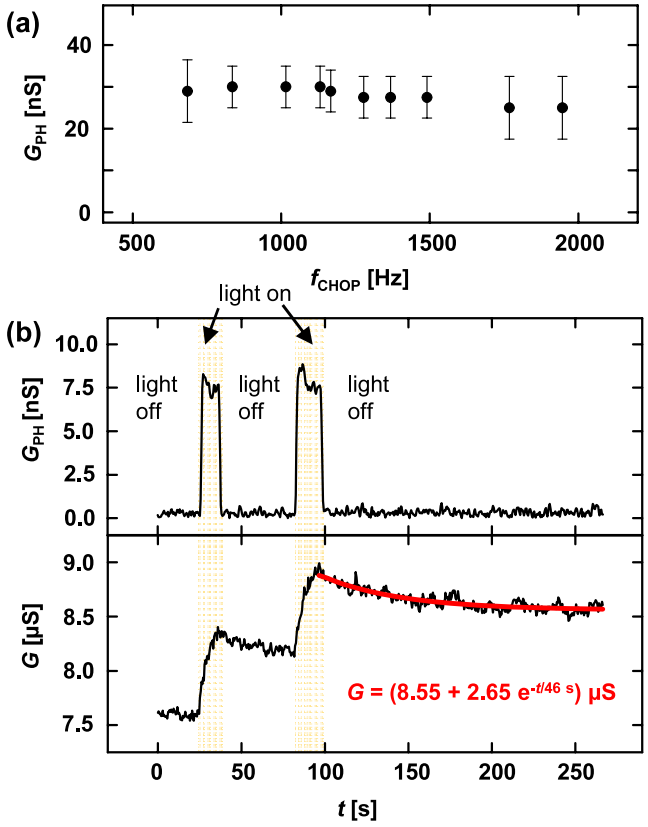

Figure 5. (a) Typical frequency dependence of the photoconductance of the PSI–CNT hybrids in the kHz regime at $I_{\mathrm{LASER}} = 17$ kW cm^{-2} at room temperature. (b) Upper graph: photoconductance G_{PH} of the PSI–CNT hybrids as a function of the laboratory time t ($f_{\mathrm{CHOP}} = 1.1$ kHz). Lower graph: conductance G measured at the same time as the upper graph. The line is an exponential fit to the data with a typical time constant of several seconds.

4. Discussion

The data in figures 4(c) and (d) demonstrate that the PSI–CNT hybrid material exhibit a strongly enhanced photoconductance signal at photon wavelengths close to the absorption maxima of the PSI compared to non-resonant wavelengths. In addition, the control samples of purified CNTs do not show such an enhanced photoconductance signal (figures 4(a) and (b)). The data in figure 3(b) further verifies that the conductance change G in the CNTs is induced by optically excited PSI

proteins, which are bound to the CNTs. Therefore, the results demonstrate that an electronically active junction is formed between the PSI and the CNTs, which influences the photoconductance of the CNTs. The PSI–CNT hybrids exhibit a unique topology in which the oxidizing side of the PSI is oriented towards the CNTs. Hereby, the excitation of the PSI by light induces a vectorial charge separation perpendicular to the CNTs' surface. The electron is transferred along the electron transfer chain of the reaction center (figure 1(a)), leaving a hole at the oxidizing side of the PSI which is coupled to the CNT surface. It is therefore likely that the change in the photoconductance of the PSI–CNT hybrids is caused by the optically excited hole which tunnels into the CNTs. Such a charge transfer gives rise to a change of the charge density n and, in turn, a change of the conductance G of the CNTs ($G \propto \sigma = nq_e\mu$, with σ the conductivity of the CNTs, n the charge carrier density of the CNTs, μ the carrier mobility of the CNTs and q_e the electron charge). In this scenario, the optically excited electron stays at the final acceptor within the PSI until it eventually recombines with the spatially separated hole. Most importantly, this interpretation explains the long timescale of the optically induced conductance change in the lower graph of figure 5(b) in a way that the timescale reflects the recombination of the spatially separated charge carriers. We note that the optically excited electron needs to stay on the PSI, since the photoconductance measurements are performed in vacuum. Hereby, a net charge transfer from the CNTs via the PSI to the environment can be neglected. A further interpretation, in which the hole resides inside the PSI with no charge transfer to the CNT, is also unlikely, since such an overall optoelectronic process would have a time constant which is comparable to the recombination time of electron–hole excitations in pristine PSI in the order of milliseconds [1]. This is not the case for the hybrid system as verified by the data presented in figure 5(a). Therefore, the presented results indicate the formation of an electronically active junction which mediates a vectorial light-induced charge transfer between the bound PSI and the CNTs. Further experimental and theoretical work is underway to determine the specific factors that govern charge transfer dynamics in the PSI–CNT hybrids.

5. Conclusion

Genetically varied PSI proteins containing cysteine residues at specific sites on the luminal interface are utilized to construct hybrid protein junctions with a unique topology. The proteins are covalently bound to the CNTs with the oxidizing side of the PSI oriented facing the CNTs. The system demonstrates intriguing optoelectronic properties which emerge from the formation of an active electronic junction between the PSI and the CNTs. In particular, we observe a photoconductive gain effect which follows the absorbance spectrum of the PSI. The study demonstrates that the PSI–CNT hybrids act as nanosized optical components which have the potential to serve as optical switches, nanoscale solar cells and sensors for light.

Acknowledgments

We thank L Frolov, S Richter, C Carmeli and J P Kotthaus for fruitful discussions and support. We gratefully acknowledge financial support within the DFG Priority Program 1243 (Ho 3324/2), SFB 486, the Center for NanoScience (CeNS), the LMUexcellence program and the German excellence initiative via the 'Nanosystems Initiative Munich' (NIM).

References

[1] Brettel K 1997 *Biochim. Biophys. Acta* **1318** 322
[2] Carmeli I, Frolov L, Carmeli C and Richter S 2007 *J. Am. Chem. Soc.* **129** 12353
[3] Carmeli I, Mangold M, Frolov L, Zebli B, Carmeli C, Richter S and Holleitner A W 2007 *Adv. Mater.* **19** 3901
[4] Frolov L, Rosenwaks Y, Carmeli C and Carmeli I 2005 *Adv. Mater.* **17** 2434
[5] Giardi M T and Pace E 2005 *Trends Biotechnol.* **23** 257
[6] Das R *et al* 2004 *Nano Lett.* **4** 1079
[7] Lebedev N, Trammell S A, Spano A, Lukashev E, Griva I and Schnur J 2006 *J. Am. Chem. Soc.* **128** 12044–5
[8] Frolov L, Rosenwaks Y, Richter S, Carmeli C and Carmeli I 2008 *J. Phys. Chem.* C **112** 13426–30
[9] Avouris P, Chen Z and Perebeinos V 2007 *Nat. Nanotechnol.* **2** 605–15
[10] Dresselhaus M S, Dresselhaus G and Eklund P C 1996 *Science of Fullerenes and Carbon Nanotubes* (New York: Academic)
[11] Hazani M, Naaman R, Hennrich R and Kappes M M 2003 *Nano Lett.* **3** 153
[12] Haremza J M, Hahn M A, Krauss T D, Chen S and Calcines J 2002 *Nano Lett.* **2** 1253
[13] Hazani M, Hennrich F, Kappes M, Naaman R, Peled D, Sidorov V and Shvartz D 2004 *Chem. Phys. Lett.* **391** 389
[14] Banerjee S and Wong S S 2002 *Nano Lett.* **2** 195
[15] Ravindran S, Chaudhary D, Colburn B, Ozkan M and Ozkan C S 2003 *Nano Lett.* **3** 447
[16] Guldi D M, Rahman G M A, Sgobba V and Ehli C 2006 *Chem. Soc. Rev.* **35** 471–87
[17] Tasis D, Tagmatarchis N, Bianco A and Prato M 2006 *Chem. Rev.* **106** 1105–36
[18] Lee J, Govorov A O and Kotov N 2005 *Nano Lett.* **5** 2063–9
[19] Juarez B H, Klinke C, Kornowski A and Weller H 2007 *Nano Lett.* **7** 3564–8
[20] Zebli B, Vieyra H A, Carmeli I, Hartschuh A, Kotthaus J P and Holleitner A W 2009 *Phys. Rev.* B **79** 205402
[21] Wong S S, Joselevich E, Woolly A T, Cheung C L and Lieber C M 1998 *Nature* **394** 52
[22] Balasubramanian K, Burghard M, Kern K, Scolari M and Mews A 2005 *Nano Lett.* **5** 507–10
[23] Hernández-Martínez P L and Govorov A O 2008 *Phys. Rev.* B **78** 035314
[24] Chen R J, Franklin N R, Kong J, Cao J, Tombler T W, Zhang Y and Dai H 2001 *Appl. Phys. Lett.* **79** 2258
[25] Freitag M, Martin Y, Misewich J A, Martel R and Avouris P 2003 *Nano Lett.* **3** 1067
[26] Wu Z *et al* 2004 *Science* **305** 1273
[27] Barone P W, Baik S, Heller D A and Strano M S 2005 *Nat. Mater.* **4** 86
[28] Fujiwara A, Matsuoka Y, Suematsu H, Ogawa N, Miyano K, Kataura H, Maniwa Y, Suzuki S and Achiba Y 2001 *Japan. J. Appl. Phys.* **40** L1229
[29] Qiu X, Freitag M, Perebeinos V and Avouris P 2005 *Nano Lett.* **5** 749
[30] Avouris P, Freitag M and Perebeinos V 2008 *Nat. Photon.* **2** 341–50

[31] Itkis M E, Borondiks F, Yu A and Haddon R C 2006 *Science* **312** 413
[32] Yakobson B I and Smalley R E 1997 *Am. Sci.* **85** 324
[33] Ajayan P M 1999 *Chem. Rev.* **99** 1787
[34] Dai H J 2002 *Surf. Sci.* **500** 218
[35] Frank S, Poncharal P, Wang J L and deHeer W A 1998 *Science* **280** 1744
[36] Saito Y, Hamaguchi K, Uemura S, Uchida K, Tasaka Y, Ikazaki F, Yumura M, Kasuya A and Nishina Y 1998 *Appl. Phys.* A **67** 95
[37] Fan S S, Chapline M G, Franklin N R, Tombler T W, Cassell A M and Dai H J 1999 *Science* **283** 512
[38] Lee Y H *et al* 2001 *Adv. Mater.* **13** 1371
[39] Fuhrer M S *et al* 2000 *Science* **288** 494
[40] Smorodin T, Beierlein U and Kotthaus J P 2005 *Nanotechnology* **16** 1123
[41] Guo X *et al* 2006 *Science* **311** 356
[42] Guo X, Gorodetsky A, Hone J, Barton J and Nuckolls C 2008 *Nat. Nanotechnol.* **3** 163
[43] Song L, Holleitner A W, Qian H, Hartschuh A, Döblinger M, Weig E M and Kotthaus J P 2008 *J. Phys. Chem.* B **112** 9644
[44] Kataura H, Kumazawa Y, Maniwa Y, Umezu I, Suzuki S, Ohtsuka Y and Achiba Y 1999 *Synth. Met.* **103** 2555–8